Biointerface Research in Applied Chemistry
Open-Access Journal (ISSN: 2069-5837)

Article
Volume 15, Issue 3, 2025, 33
https://doi.org/10.33263/BRIAC153.033

Tailoring Nanosensor Devices for Ion Detection in Contaminated Water by Ga–N Nanomaterials Towards a Sustainable Future

Fatemeh Mollaamin [1,*]

[1] Department of Biomedical Engineering, Faculty of Engineering and Architecture, Kastamonu University, Kastamonu, Turkey
* Correspondence: fmollaamin@kastamonu.edu.tr;

Received: 16.03.2025; Accepted: 10.05.2025; Published: 7.06.2025

Abstract: The aim of this research is to remove metal/loid ions of Na^+, K^+, Sn^{2+}, Pb^{2+}, Al^{3+}, and As^{3+} from water due to nanomaterial-based gallium nitride nanocage (Ga–N). The electromagnetic and thermodynamic attributes of metal/loid cations trapped Ga–N were depicted by materials modeling. The encapsulation of metal/loid cations occurs via chemisorption. It has been studied the behavior of trapping of main group cations of Na^+, K^+, Sn^{2+}, Pb^{2+}, Al^{3+}, As^{3+} by GaN–nc for sensing the water metal cations. Ga–N was modeled in the presence of metal/loid cations (Na^+, K^+, Sn^{2+}, Pb^{2+}, Al^{3+}, As^{3+}). Sample characterization was performed using CAM–B3LYP/EPR–3, LANL2DZ level of theory. The electric potential parameters extracted from NQR analysis have illustrated that the uptake of free potassium and sodium ions has been known to be associated with Ga–N, indicating that the K^+ and Na^+ ions encapsulated in this kind of nanocage can be internalized through a different pathway from other metal cations. Furthermore, the nuclear magnetic resonance (NMR) analysis indicated the notable peaks surrounding metal elements of Na^+, K^+, Sn^{2+}, Pb^{2+}, Al^{3+}, and As^{3+} through the trapping in the Ga–N during ion detection and removal from water; however, it can be seen some fluctuations in the chemical shielding treatment of isotropic and anisotropy tensors. Based on the results of this research, the selectivity of metal ion adsorption by Ga–N (ion sensor) has been approved as $K^+ > Na^+ > > > As^{3+} > Sn^{2+} \approx Pb^{2+} > Al^{3+}$. Finally, it has been shown that for a given number of nitrogen donor sites in Ga–N, the stabilities of monovalent (M^+), divalent (M^{2+}) and trivalent (M^{3+}) cation complexes are $K^+\Xi$Ga–N > $Na^+\Xi$Ga–N >>> $As^{3+}\Xi$Ga–N > $Sn^{2+}\Xi$Ga–N ≈ $Pb^{2+}\Xi$Ga–N > $Al^{3+}\Xi$Ga–N. In this article, it is proposed that metal/loid cations–adsorbed can be used to decorate and enlarge the optoelectronic properties of Ga–N, which can be used to produce photoelectric devices for water treatment.

Keywords: Ion detector; water contamination, gallium nitride nanostructure; computational method.

1. Introduction

Water is one of the most important natural resources. It is an essential substance for life and is considered a universal solvent capable of dissolving almost all solutes. Additionally, water is widely used in households, agriculture, industry, and tourism, and therefore, water conservation should be a basic human need. The chemical characteristics of natural waters reflect the soils and rocks that have been in contact with water. The quality and quantity of the chemical elements in surface waters are affected by the geochemical structure of the surrounding area, land use, seasonal variations of weather conditions, vegetation, and atmospheric deposits [1,2].

The researchers have investigated the selectivity and priority of metal removal based on the type of surfactant in foam separation [3–5]. In general, according to Hoffmeister's series, it has been reported that alkali metals with smaller atomic numbers are more likely to precipitate with carboxylic acid in aqueous solutions [6–8]. The Hoffmeister's series was derived from the results of the protein salting-out effects ($Li^+ > Na^+ > K^+ > Rb^+ > Cs^+$). By contrast, micelles of surfactants with sulfate groups have a higher degree of binding of counterion with alkali metals of higher atomic numbers ($Li^+ < Na^+ < K^+ < Rb^+ < Cs^+$) [9].

The quantity and quality of the chemical atoms in surface waters are impacted by a geochemical combination of environment, soil use, changes in seasonal climate, vegetation, and atmospheric conditions [10–14].

These days, atmospheric contaminations caused by toxic organic compounds and hazardous metal/loid, with their persistence, are a serious obstacle worldwide [15]. For instance, lead (Pb) is a heavy metal that exists abundantly in the environment. The improvement of lifestyle and dependent productions enhanced the value of lead emissions and made explicit growth in doping in the surrounding area [16, 17]. Lead does not decompose in the environment, so it collects in the living cells and poses a high health hazard [18,19]. Newly, an overview of the potential of magnetite nanoparticles and their composites to behave in polluted water and scavenge unpleasant contaminations has been represented [20].

Rybarczyk and his co-workers have remarked on the consequences of experiments about the synchronic elimination of Al (III), Cu (II), and Zn (II) from dilute aqueous solutions applying ion and sudden flotation approaches. The concluded data have been exhibited through physicochemical areas dependent on metal salts in aqueous solutions [21].

In addition, the element of tin (Sn) is a grey and white metal and appears in the oxidation states of Sn^{2+} and Sn^{4+} cations. Recently, Rathinam *et al.* have prepared the structurally isomeric rhodamine 6G-based amino derivatives for detecting Sn^{2+} cations [22].

The researchers have investigated the priority and selectivity of metal grabbing on the basis of the nature of surfactant in foam separation [23–25]. Generally, pursuant to Hoffmeister's series, it was announced that first-group metals with lower atomic numbers are precipitated with carboxylic acid (R-COOH) in watery solutions [26–28].

The gallium nitride (GaN) molecule is one of the most explored of the third group semiconductors containing nitrogen elements, which are employed in various applications such as detector tools and optoelectronic and electronic instruments [29–32]. Regarding the important electronic attributes of GaN, it can be a suitable sample for gas detection [33–35]. In addition, density function theory (DFT) can be applied to investigate the mechanisms of complexes and adsorption reactions [36–39]. The application of DFT in the adsorption reaction system is summarized in this paper.

Compared to past semiconductor substances, 3D-GaN is a broad-band gap semiconductor system [40]. Therefore, it can empower instrument operation at high frequency/voltage or temperature, indicating high luminous yield, proper thermal conduction, high-temperature persistence, stability to acids and alkalis, and anti-radiation attributes [41]. The adsorption of elements on the solid surface might interact indirectly through elastic distortion of the substrate or electron scattering with a long-range atomic interaction adjusted by the substrate, which runs a significant function in the self-assembly atomic shape. Since alkali metal elements might lightly miss electrons, their adsorption on the semiconducting nanomaterials might change them to n-type, which will, in turn, decrease their effective action and alter their optoelectronic attributes [42]. Recently, many researchers have announced verdicts on the optoelectronic attributes of alkali-metal-adsorbed two-dimensional materials [43–53]. The alkali-metal atoms adsorbing on graphene [43,44] and g-GaN [54] applying a first-principles approach has been studied, and it has been discovered that the optoelectronic specifications of graphene and g-GaN are improved by the alkali-metal adsorbing.

The density amount of Ga–N material is approximately low. Therefore, it is envisaged to develop the limitation of contaminants and dominate the weak adsorption, quick compression, and secondary pollution in the modification technology. As a matter of fact, the target of this research is to trap the cations of Na^+, K^+, Sn^{2+}, Pb^{2+}, Al^{3+}, and As^{3+} in the water phase. This article investigates the removal of heavy metal ions from wastewater, which is of prime importance for a clean environment and human health. Different reported methods were devoted to removing heavy metal ions from various wastewater sources.

2. Materials and Methods

2.1. Metal/metalloid cations captured in Ga–N.

The aim of this study is to remove alkali and alkaline earth metal cations from water by using Ga–N. The intention is to remove Na^+, K^+, Sn^{2+}, Pb^{2+}, Al^{3+}, and As^{3+} from the aqueous solution containing a group of alkali and alkaline earth metals. The model solution is composed of the target of an alkali/alkaline earth metal and the Ga–N in an aqueous solution (Figure 1). Gallium nitride nanocage was modeled in the presence of metal cations (Na^+, K^+, Sn^{2+}, Pb^{2+}, Al^{3+}, As^{3+}). Roy *et al*. have calculated alkali and alkaline earth metal derivatives of COT due to CAM-B3LYP functional [55]. CAM-B3LYP yields atomization energies of similar quality to those from B3LYP while also performing well for charge transfer excitations, which B3LYP underestimates enormously. In our research, sample characterization was performed using CAM–B3LYP/EPR–3, LANL2DZ level of theory.

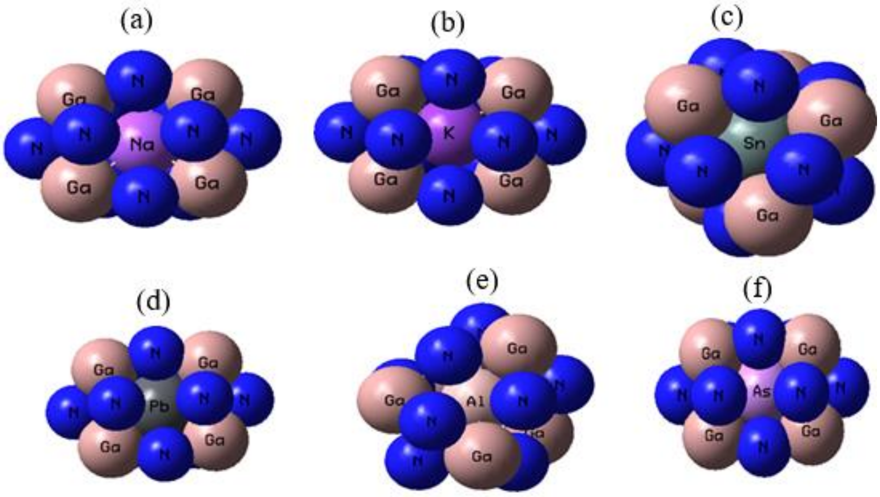

Figure 1. Adsorption of metal/loid ions (Na^+, K^+, Sn^{2+}, Pb^{2+}, Al^{3+}, As^{3+}) from drinking water by Ga–N trough formation of **a)** Na^+ΞGa–N; **b)** K^+ΞGa–N; **c)** Sn^{2+}ΞGa–N; **d)** Pb^{2+}ΞGa–N; **e)** Al^{3+}ΞGa–N; **f)** As^{3+}ΞGa–N complexes toward water purification technology.

Figure 1 shows the process of ion-trapping containing alkali and alkaline earth metal ions (Na^+, K^+, Sn^{2+}, Pb^{2+}, Al^{3+}, As^{3+}) which exist in the periodic box of water molecules towards the formation of MCs complexes by molecular modeling computations.

The charge distribution of Li^{+}ΞGa–N, Na^{+}ΞGa–N, K^{+}ΞGa–N, Be^{2+}ΞGa–N, Mg^{2+}ΞGa–N and Ca^{2+}ΞGa–N complexes is calculated due to the Bader charge analysis [56].

The metal cations were successfully incorporated in the center of Ga–N towards the formation of Li^{+}ΞGa–N, Na^{+}ΞGa–N, K^{+}ΞGa–N, Be^{2+}ΞGa–N, Mg^{2+}ΞGa–N, and Ca^{2+}ΞGa–N complexes (Figure 1). Regardless of which metal, the Gallium nitride nanocage expanded to accommodate the metal particles. By using mixtures of metal nanoparticles of two different sizes, it was found that the inclusion and the resultant pore size were controlled by the larger size metal particles (Figure 1).

2.2. Density functional theory (DFT) approach.

Our computations have been carried out due to the conceptual DFT using the projector–augmented–wave (PAW) methodology [57]. The Perdew–Burke–Ernzerhof (PBE) functional under the generalized gradient approximation (GGA) was applied as the exchange-correlation functional [58]. The non-empirical PBE functional is recognized to relegate precise crystal specifications [59]. Commonly, where GGA functionals lose out, local density functionals stop, too. Considering the thermal conductivity compared to local density functionals, PBE does not over-attach structures; therefore, the interatomic force constants are not too flexible. All in all, the lattice thermal conductivity is the same whether using local density or GGA functionals [60].

Hohenberg-Kohn (HK) functions have rigidly made electronic density permissible as a fundamental variable in electronic and structure computations. In other words, the development of the applied DFT methodology only became notable after W. Kohn and L. J. Sham released their reputable series of equations, which were introduced as Kohn-Sham (KS) equations [61, 62].

Considering the electronic density within the KS image, we are able to see a remarkable reduction in quantum computing. Thus, the KS methodology lightens the route for pursuing systems that cannot be discussed by conventional ab initio methodologies. Kohn and Sham" introduce the solution, which brings up the mono-electronic orbitals to account for the kinetic energy in a simple and relatively exact by finding a residual modification that might be computed apart. So, one starts with a reference model of M with non-interacting electrons related to the external potential v_s and with Hamiltonian [61, 62]:

$$\hat{H}_s = -\sum_i^M \frac{1}{2}\nabla_i^2 + \sum_i^M v_s(\vec{r}_i) = \sum_i^M \hat{h}_s \qquad (1)$$

$$\hat{h}_s = -\frac{1}{2}\nabla_i^2 + v_s(\vec{r}_i) \qquad (2)$$

By representing the single-particle orbitals ψ_i all electronic densities physically acceptable for the system of "non-interacting" electrons are written in the equation (3):

$$\rho(\vec{r}) = \sum_i^M |\psi_i(\vec{r})|^2 \quad (3)$$

Finally, the total energy could be measured by the KS method due to the equation (4):

$$E[\rho] = \sum_i^M n_i \left\langle \psi_i \left| -\frac{1}{2}\nabla^2 + v_{ext}(\vec{r}) + \frac{1}{2}\int \frac{\rho(\vec{r}\,')}{|\vec{r}-\vec{r}\,'|}\,\mathrm{d}\vec{r}\,' \right| \psi_i \right\rangle + E_{xc}[\rho] + \frac{1}{2}\sum_{\beta}^{N}\sum_{\alpha\neq\beta}^{N} \frac{Z_\alpha Z_\beta}{|\vec{R}_\alpha - \vec{R}_\beta|} \qquad (4)$$

Therefore, the precise exchange energy function is described by the Kohn–Sham orbitals in lieu of the density, which is cited as the indirect density functional. This research has employed the penetration of the hybrid functional of a three-parameter basis set of B3LYP (Becke, Lee, Yang, Parr)" within the conception of DFT upon theoretical computations [63, 64]. The popular B3LYP (Becke, three-parameter, Lee–Yang–Parr) and exchange-correlation functional becomes based on equation (5) [65–67]:

$$E_{\mathrm{XC}}^{\mathrm{B3LYP}} = (1-\alpha)E_{\mathrm{x}}^{\mathrm{LSDA}} + \alpha E_{\mathrm{x}}^{\mathrm{HF}} + b\Delta E_{\mathrm{x}}^{\mathrm{B}} + (1-c)E_{c}^{\mathrm{LSDA}} + cE_{c}^{\mathrm{LYP}} \qquad (5)$$

$\alpha = 0.20, b = 0.72, c = 0.81$ shows a generalized gradient approximation: the Becke exchange functional [68] and the correlation functional of Lee *et al*. [69] for B3LYP and $E_{\mathrm{c}}^{\mathrm{LSDA}}$ is the VWN local spin density approximation to the correlation functional [70].

In this article, the rigid PES using DFT calculations was accomplished using the Gaussian 16 revision C.01 program package [71]. The input Z-matrix for encapsulation of the metal cations (Na^+, K^+, Sn^{2+}, Pb^{2+}, Al^{3+}, As^{3+}) in water by the Ga–N has been provided with GaussView 6.1 [72] due to the rigid system and coordination format of which a blank line has been cited and using LANL2DZ basis set to distinguish chemical shielding, frequencies, thermodynamic properties, electrostatic and electronic potential, natural atomic charges, projected density of state and other quantum properties for this work. In this study, the interaction between metal ions and Ga–N was modeled and analyzed. As revealed by DFT-based analysis, the ability of Ga–N to grab metal ions was determined mainly by the electronegativity of the functional groups, the electronegativity of the metals, and the ionic radius of the metals, as well as the interaction between Ga–N and the metals.

NQR is a straight frame of the interaction of the quadrupole moment with the EFG, which is produced by the electronic structure of its ambiance. Therefore, the NQR transition frequencies are symmetric to the electric quadrupole moment of the nucleus and a measurement of the strength of the local EFG [73, 74]. The NQR method is related to the multipole expansion in Cartesian coordinates as the equation (6):

$$V(r) = V(0) + \left[\left(\frac{\partial V}{\partial x_i}\right)\Big|_0 . x_i\right)\Big] + \frac{1}{2}\left[\left(\frac{\partial^2 V}{\partial x_i x_j}\right)\Big|_0 . x_i x_j\right)\Big] + \cdots \qquad (6)$$

After that, a simplification on the equation (6), there are only the second derivatives related to the identical variable for the potential energy [73, 74]:

$$U = -\frac{1}{2}\int_{\mathcal{D}} d^3\, r\, \rho_r \left[\left(\frac{\partial^2 V}{\partial x_i^2}\right)\Big|_0 . x_i^2\right)\Big] = -\frac{1}{2}\int_{\mathcal{D}} d^3\, r\, \rho_r \left[\left(\frac{\partial E_i}{\partial x_i}\right)\Big|_0 . x_i^2\right)\Big] = -\frac{1}{2}\left(\frac{\partial E_i}{\partial x_i}\right)\Big|_0 . \int_{\mathcal{D}} d^3\, r\, [\rho(r). x_i^2] \qquad (7)$$

There are two parameters that must be obtained from NQR experiments: the quadrupole coupling constant, χ, and the asymmetry parameter of the EFG tensor η:

$$\chi = {e^2 Q q_{zz}}/{h} \qquad (8)$$

$$\eta = {q_{xx} - q_{yy}}/{q_{zz}} \qquad (9)$$

where q_{ii} are ingredients of the EFG tensor at the quadrupole nucleus determined in the EFG principal axes system, Q is the nuclear quadrupole moment, e is the proton charge, and h is the Planck's constant [75,76].

3. Results and Discussion

Element cations that are dominant in water are alkali and alkaline earth metal cations (Na^+, K^+, Sn^{2+}, Pb^{2+}, Al^{3+}, As^{3+}). The data evaluated the efficiency of gallium nitride nanocage (Ga–N) for metal cation encapsulation. In fact, the chemisorptive nature of the bond among the metal cations with gallium and nitrogen elements can be remarked on through the equilibrium distribution of metal cations, Ga–N, and a monolayer attribute.

3.1. Nuclear quadrupole resonance (NQR) analysis.

In this research, the calculated nuclear quadrupole resonance/NQR specifications extracted from electrostatic properties have been calculated for the trapping of first and second main group metal cations including Na^+, K^+, Sn^{2+}, Pb^{2+}, Al^{3+}, As^{3+} in Ga–N which is accord to the results of the nuclear quadrupole moment, a trait of the nucleus, and the electric field gradient/EFG in the neighborhood of the nucleus.

As the EFG at the citation of the nucleus in metal cations including Na^+, K^+, Sn^{2+}, Pb^{2+}, Al^{3+}, As^{3+} is allocated by the valence electrons twisted in the particular attachment with close nuclei of Ga–N through trapping of metal cations, the NQR frequency at which transitions occur is particular for (Na^+, K^+, Sn^{2+}, Pb^{2+}, Al^{3+}, As^{3+})ΞGa–N complexes (Table 1).

In this research work, the electric potential as the quantity of work energy through carrying over the electric charge from one position to another position in the essence of electric field has been evaluated for Na^+ΞGa–N, K^+ΞGa–N, Sn^{2+}ΞGa–N, Pb^{2+}ΞGa–N, and Al^{3+}ΞGa–N and As^{3+} Ξ Ga–N complexes using CAM–B3LYP/EPR–3, LANL2DZ level of theory (Table1).

Table 1. The electric potential (a.u.) and Bader charge (e) through NQR calculation for Na^+ΞGa–N, K^+ΞGa–N, Sn^{2+}ΞGa–N, Pb^{2+}ΞGa–N, and Al^{3+}ΞGa–N and As^{3+}ΞGa–N complexes using CAM-B3LYP/EPR–3, LANL2DZ calculation.

Na^+ΞGa–N			**K^+ΞGa–N**			**Sn^{2+}ΞGa–N**		
Atom	**Q**	**E_p**	**Atom**	**Q**	**E_p**	**Atom**	**Q**	**E_p**
Ga1	0.8788	–146.607	Ga1	0.8743	–146.572	Ga1	0.5623	–1.1730
N2	–0.4796	–18.164	N2	–0.4628	–18.17	N2	–0.4772	–18.4139
N3	–0.5117	–18.1776	N3	–0.5362	–18.187	N3	–0.5985	–18.4361
Ga4	0.8820	–146.6	Ga4	0.8372	–146.568	Ga4	0.5647	–1.175
Ga5	0.8676	–146.627	Ga5	0.8698	–146.608	Ga5	0.5867	–1.1762
Ga6	0.8846	–146.63	Ga6	0.8979	–146.606	Ga6	0.5684	–1.1717
N7	–0.4655	–18.1578	N7	–0.4479	–18.1622	N7	–0.4746	–18.4082
N8	–0.5121	–18.1756	N8	–0.5369	–18.1746	N8	–0.5907	–18.4378
N9	–0.493	–18.184	N9	–0.5128	–18.1942	N9	–0.4921	–18.4055
N10	–0.4899	–18.1751	N10	–0.5009	–18.1839	N10	–0.4772	–18.4002
N11	–0.4725	–18.1723	N11	–0.4849	–18.1807	N11	–0.4848	–18.4053
N12	–0.5400	–18.1888	N12	–0.5741	–18.2027	N12	–0.5148	–18.4203
Ga13	0.9325	–146.616	Ga13	0.8611	–146.618	Ga13	0.5321	–1.1145
N14	–0.4540	–18.1331	N14	–0.4503	–18.1287	N14	–0.4500	–18.3964
N15	–0.4464	–18.1317	N15	–0.4401	–18.1276	N15	–0.4411	–18.3895
Na16	0.4193	–34.5186	**K16**	0.6067	–74.29	**Sn16**	2.1869	–1.3890
Pb^{2+} Ξ Ga–N			Al^{3+} Ξ Ga–N			As^{3+} Ξ Ga–N		
Atom	Q	E_p	Atom	Q	E_p	Atom	Q	E_p
Ga1	0.6030	–1.1721	Ga1	0.5971	–1.2004	Ga1	0.7196	–1.18992
N2	–0.4980	–18.4213	N2	–0.4584	–18.4	N2	–0.5008	–18.4167
N3	–0.5607	–18.4446	N3	–0.5471	–18.4188	N3	–0.6600	–18.43
Ga4	0.5885	–1.1734	Ga4	0.6131	–1.2019	Ga4	0.7179	–1.1905
Ga5	0.6239	–1.1770	Ga5	0.6331	–1.2042	Ga5	0.7436	–1.1930
Ga6	0.5969	–1.1715	Ga6	0.6015	–1.2014	Ga6	0.7148	–1.1894
N7	–0.4882	–18.4154	N7	–0.4624	–18.3963	N7	–0.4854	–18.4186
N8	–0.5576	–18.4477	N8	–0.5505	–18.4235	N8	–0.6530	–18.4308
N9	–0.5151	–18.4193	N9	–0.4786	–18.4124	N9	–0.4783	–18.399
N10	–0.5150	–18.4283	N10	–0.4673	–18.412	N10	–0.4647	–18.3968
N11	–0.5064	–18.4244	N11	–0.4771	–18.4151	N11	–0.4746	–18.4008

N12	–0.5282	–18.438	N12	–0.5020	–18.4259	N12	–0.5175	–18.4045
Ga13	0.6256	–1.1201	Ga13	0.42170	–1.1787	Ga13	0.6182	–1.1346
N14	–0.4340	–18.3897	N14	–0.4300	–18.3822	N14	–0.4642	–18.4111
N15	–0.4411	–18.3841	N15	–0.4226	–18.3808	N15	–0.4613	–18.4034
Pb16	2.0066	–1.3702	**Al16**	1.9296	–1.0981	**As16**	1.6458	–2.2729

In Table 1, the Bader charge and electronic potential properties of different atoms of Ga, N, and metal and metalloid ions of Na^{+}, K^{+}, Sn^{2+}, Pb^{2+}, Al^{3+}, and As^{3+} trapped on the Ga–N have been investigated. The amounts indicate that with increasing the negative charge of different atoms, the electric potential resulting from NQR calculations increases. Moreover, the most negative charges belong to Na^{+} in Na$^{+}\Xi$Ga–N complex (electron acceptor), which approves the most electron transfer from nitrogen (electron donor) in Ga–N to metal ion (Table 1).

Furthermore, in Figure 2 (a–f), it has been sketched the electric potential of nuclear quadrupole resonance for some atoms of (Na^{+}, K^{+}, Sn^{2+}, Pb^{2+}, Al^{3+}, As^{3+}) in the trapping in the Ga–N through metal cations adsorption which has been calculated by CAM–B3LYP/EPR–3, LANL2DZ.

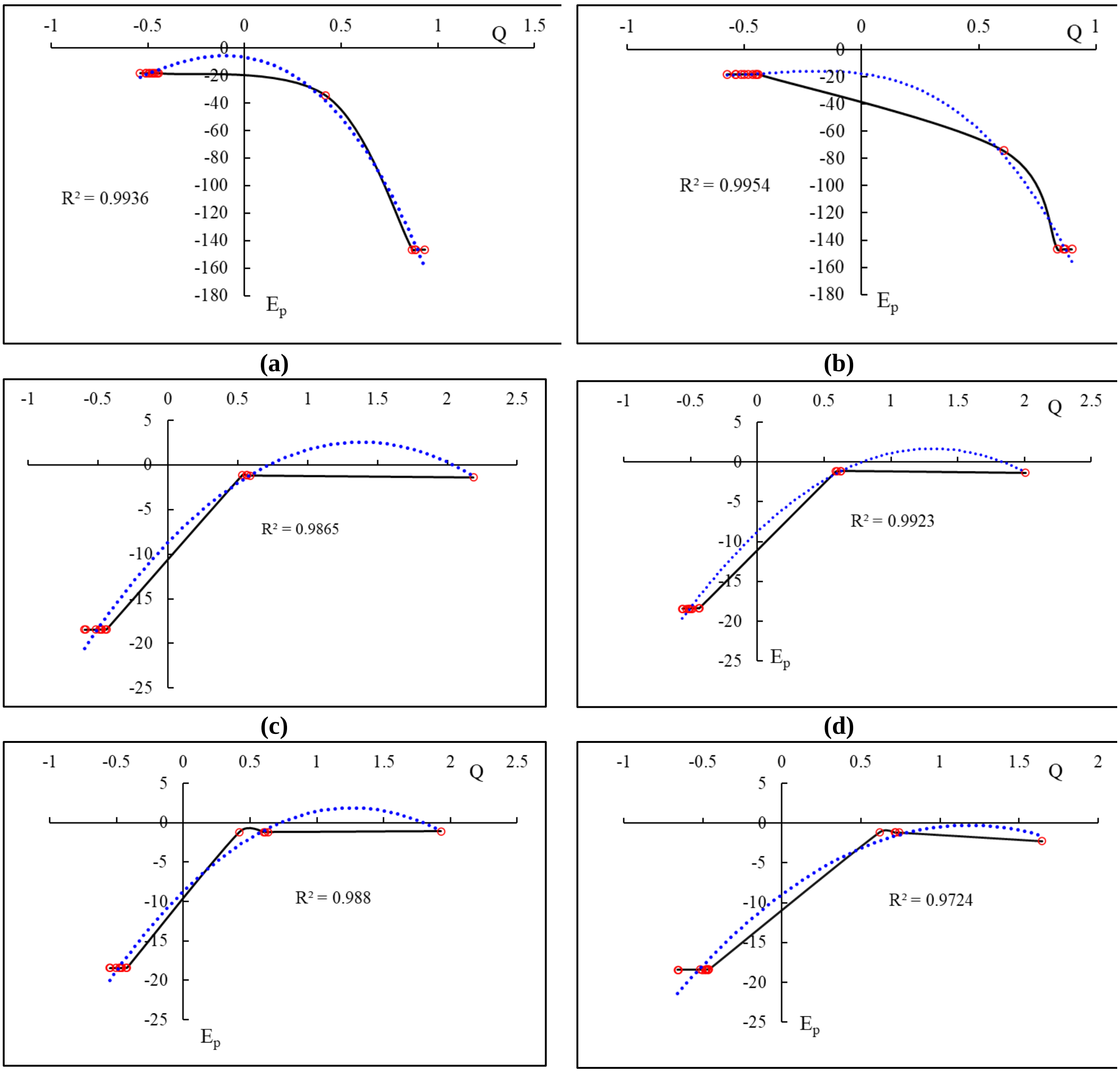

(a) (b)

(c) (d)

(e) (f)

Figure 2. Electric potential (a.u.) versus Bader charge (e) through NQR calculation for **(a)** Na$^{+}\Xi$Ga–N; **(b)** K$^{+}\Xi$Ga–N; **(c)** Sn$^{2+}\Xi$Ga–N; **(d)** Pb$^{2+}\Xi$Ga–N; **(e)** Al$^{3+}\Xi$Ga–N; **(f)** As$^{3+}\Xi$Ga–N complexes by CAM–B3LYP/EPR–3, LANL2DZ.

In Figure 2 (a–f), the behavior of trapping of main group cations of Na^{+}, K^{+}, Sn^{2+}, Pb^{2+}, Al^{3+}, and As^{3+} by gallium nitride nanocage for sensing the water metal cations was observed. It’s vivid that the curve of Ga–N is waved by these metal cations. The sharpest peaks for electric potential have been shown around metal cations trapping on Ga–N, which present the electron-accepting characteristics of these atoms versus the gallium and nitrogen atoms of Ga–N (Figure 2a–f).

The ions of Na^{+} and K^{+} in Na^{+}ΞGa–N (Figure 2a) and K^{+}ΞGa–N (Figure 2b), respectively, have shown approximately the same behavior with the relation coefficients of $R^2_{Na^+}$= 0.9954 and $R^2_{K^+}$ = 0.9954. Furthermore, Sn^{2+} in Sn^{2+}ΞGa–N (Figure2c), Pb^{2+} in Pb^{2+}ΞGa–N (Figure2d), Al^{3+} in Al^{3+}ΞGa–N (Figure2e), As^{3+} in As^{3+} Ξ Ga–N (Figure2f), respectively, with relation coefficients of $R^2_{Sn^{2+}}$ = 0.9865 and $R^2_{Pb^{2+}}$= 0.9923, $R^2_{Al^{3+}}$= 0.988, $R^2_{As^{3+}}$ = 0.9724. Since potassium and sodium have electric potentials of –74.29 and –34.5186 a.u., respectively, a different fluctuation of the graph of Q versus Ep compared to tin, lead, aluminum, and arsenic has been seen (Table 1). In fact, the uptake of free potassium and sodium ions has been known to be associated with Ga–N, indicating that the potassium and sodium ions encapsulated in this kind of nanocage can be internalized through a different pathway from other metal cations.

3.2. NMR spectra analysis.

Based on resulted amounts, nuclear magnetic resonance (NMR) spectra of Ga–N as the potent sensor for adsorbing the main group cations of Na^{+}, K^{+}, Sn^{2+}, Pb^{2+}, Al^{3+}, As^{3+} can unravel the efficiency of Ga–N for detecting and removing of these metal cations in water.

From the DFT calculations, it has been attained the chemical shielding (CS) tensors in the principal axes system to estimate the isotropic chemical shielding (CSI) and anisotropic chemical shielding (CSA) [77]:

$$\sigma_{iso} = \frac{\sigma_{11} + \sigma_{22} + \sigma_{33}}{3} \qquad (10)$$

$$\sigma_{aniso} = \sigma_{33} - (\sigma_{22} + \sigma_{11})/2 \qquad (11)$$

The chemical shielding extracts from NMR can be applied for allocating the structural and geometrical specifications of materials. As a matter of fact, Gauge Invariant Atomic Orbital (GIAO) methodology has been recommended as a valid methodology for NMR parameter computations. Our own N-layered Integrated molecular Orbital and Molecular mechanics (ONIOM) has caught many regards for gaining NMR chemical shielding of gas molecule-surface complexes such as isotropic chemical shielding appears in equation (12):

$$\sigma_{iso,ONIOM} = \sigma_{iso,high(QM1)} + \sigma_{iso,medium(QM2)} + \sigma_{iso,low(QM3)} \qquad (12)$$

The NMR data of isotropic (σ_{iso}) and anisotropic shielding tensor (σ_{aniso}) of Na^{+}, K^{+}, Sn^{2+}, Pb^{2+}, Al^{3+}, As^{3+} trapped them in Ga–N towards the formation of Na^{+}ΞGa–N, K^{+}ΞGa–N, Sn^{2+}ΞGa–N, Pb^{2+}ΞGa–N, Al^{3+}ΞGa–N, and As^{3+}ΞGa–N complexes have been computed by Gaussian 16 revision C.01 program package [71] and been shown in Table2.

Table 2. Data of NMR shielding tensors for selected atoms of Na^{+}ΞGa–N, K^{+}ΞGa–N , Sn^{2+}ΞGa–N , Pb^{2+}ΞGa–N, Al^{3+}ΞGa–N , and As^{3+}ΞGa–N complexes using CAM-B3LYP/LANL2DZ calculation.

Na^{+}ΞGa–N			**K^{+}ΞGa–N**			**Sn^{2+}ΞGa–N**		
Atom	**σ_{iso}**	**σ_{aniso}**	**Atom**	**σ_{iso}**	**σ_{aniso}**	**Atom**	**σ_{iso}**	**σ_{aniso}**
Ga1	176.0442	3288.7740	Ga1	176.0442	3288.7740	Ga1	12.1048	24.7872
N2	146.2084	962.6405	N2	146.2084	962.6405	N2	261.5476	346.7223

Na^{+}ΞGa–N			**K^{+}ΞGa–N**			**Sn^{2+}ΞGa–N**		
Atom	**σ_{iso}**	**σ_{aniso}**	**Atom**	**σ_{iso}**	**σ_{aniso}**	**Atom**	**σ_{iso}**	**σ_{aniso}**
N3	559.4041	1683.7566	N3	559.4041	1683.7566	N3	218.4619	709.2896
Ga4	313.1950	3636.4504	Ga4	313.1950	3636.4504	Ga4	12.6808	19.6937
Ga5	664.6836	3206.2957	Ga5	664.6836	3206.2957	Ga5	9.9406	21.2027
Ga6	426.0429	2698.2576	Ga6	426.0429	2698.2576	Ga6	13.2415	22.7502
N7	81.1500	707.7763	N7	81.1500	707.7763	N7	194.0188	248.0492
N8	317.1902	1085.0094	N8	317.1902	1085.0094	N8	69.7006	648.1644
N9	190.4914	825.4995	N9	190.4914	825.4995	N9	224.7932	351.8422
N10	212.9765	1100.8884	N10	212.9765	1100.8884	N10	179.1911	285.8777
N11	183.1710	944.6942	N11	183.1710	944.6942	N11	313.7818	600.5299
N12	41.6829	684.3389	N12	41.6829	684.3389	N12	74.4761	269.4956
Ga13	48.8067	1547.5695	Ga13	48.8067	1547.5695	Ga13	14.3093	16.7176
N14	307.1220	507.1908	N14	307.1220	507.1908	N14	342.9848	1224.0664
N15	339.2513	700.6093	N15	339.2513	700.6093	N15	350.7752	810.5883
Na16	489.7468	66.8350	**K16**	489.7468	66.8350	**Sn16**	26.4779	9.0718
Pb^{2+}ΞGa–N			**Al^{3+}ΞGa–N**			**As^{3+}ΞGa–N**		
Atom	**σ_{iso}**	**σ_{aniso}**	**Atom**	**σ_{iso}**	**σ_{aniso}**	**Atom**	**σ_{iso}**	**σ_{aniso}**
Ga1	4.6063	14.0165	Ga1	4.8060	20.9588	Ga1	9.6900	20.2091
N2	271.9544	537.4020	N2	22.6113	589.3066	N2	109.0169	130.4181
N3	133.1549	687.9196	N3	665.5865	1248.2876	N3	122.6319	276.8316
Ga4	9.7709	15.7436	Ga4	3.5951	17.7406	Ga4	8.8143	14.2817
Ga5	4.1482	14.6684	Ga5	0.9806	20.6433	Ga5	8.5637	14.9535
Ga6	9.2320	19.2702	Ga6	2.5714	21.8420	Ga6	10.1722	18.1431
N7	327.6876	845.9131	N7	168.3817	1113.5301	N7	234.9205	203.0611
N8	75.7414	751.7755	N8	552.8558	1103.1616	N8	2.8664	192.9452
N9	140.1057	405.9991	N9	178.9364	515.8756	N9	158.8212	450.9672
N10	238.8911	205.7190	N10	199.6504	483.3784	N10	179.6835	415.2262
N11	191.9187	577.6869	N11	115.4632	597.3780	N11	153.8919	153.8919
N12	62.8760	244.3127	N12	93.8285	471.3872	N12	190.2822	243.9391
Ga13	8.3990	9.7179	Ga13	6.2769	7.1651	Ga13	9.8567	10.8558
N14	358.5329	636.8744	N14	100.0203	330.2154	N14	427.8764	960.4075
N15	486.5791	857.6936	N15	64.0987	642.4470	N15	356.7554	956.9046
Pb16	24.2002	4.5236	**Al16**	16.7175	10.2771	**As16**	35.6245	5.7157

In Table 2, NMR data has reported the notable amounts for metal cations of Na^{+}, K^{+}, Sn^{2+}, Pb^{2+}, Al^{3+}, and As^{3+}, which were trapped in the Ga–N as the selective sensor for detecting metal ions in water. The observed increase in the chemical shift anisotropy spans for Ga (4), Ga (5), and Ga (6) in Na^{+}ΞGa–N and K^{+}ΞGa–N complexes is due to Na^{+}, K^{+} ions binding to Ga–N (Figures 3a, b). The complexes of Sn^{2+}ΞGa–N (Figure 3c) and Pb^{2+}ΞGa–N (Figure 3d) have shown approximately similar behavior through the fluctuation of chemical shift anisotropy spans for functionalized atoms of N (2), N (3), N (7), N (8), N (9), N (11), N (12), N (14), N (15). Moreover, the complexes of Al^{3+}ΞGa–N (Figure 3e) and As^{3+}ΞGa–N (Figure 3f) have shown approximately similar behavior through the fluctuation of chemical shift anisotropy spans for functionalized atoms of N (2), N (3), N (7), N (8), N (9), N (14), N (15).

The observed weak signal intensity near the parallel edge of the nanocage pattern may be due to calcium or magnesium ion-binding induced non-spherical distribution of these complexes.

It is remarkable that the interaction of monovalent (M^+), divalent (M^{2+}), and trivalent (M^{3+}) cations with Ga–N promotes the stability of nanocage that results in enhanced magnetic alignment of complexes. Interestingly, the reported results show that both M^+, M^{2+}, and M^{3+} can be optimized to achieve optimal alignment of nanocage in the presence of an applied magnetic field.

In fact, the encapsulation of Na^+, K^+, Sn^{2+}, Pb^{2+}, Al^{3+}, and As^{3+} can introduce spin polarization on the (Na^+, K^+, Sn^{2+}, Pb^{2+}, Al^{3+}, As^{3+})–encapsulated Ga–N which indicates that these surfaces might be applied as magnetic energy storage. In fact, it is revealed that the isotropic and anisotropic shielding fluctuates with the occupancy in the electron-accepting metal cations trapped in the gallium nitride nanocage.

Figure 3 exhibited the same tendency of shielding for gallium and nitrogen; however, a considerable deviation exists from metal cations (electron acceptor) of Na16 (Figure 3a), K16 (Figure 3b), Sn16 (Figure 3c), Pb16 (Figure 3d), Al16 (Figure 3e), and As16 (Figure 3f) through interaction with nitrogen atoms (electron donner) during trapping in the Ga–N.

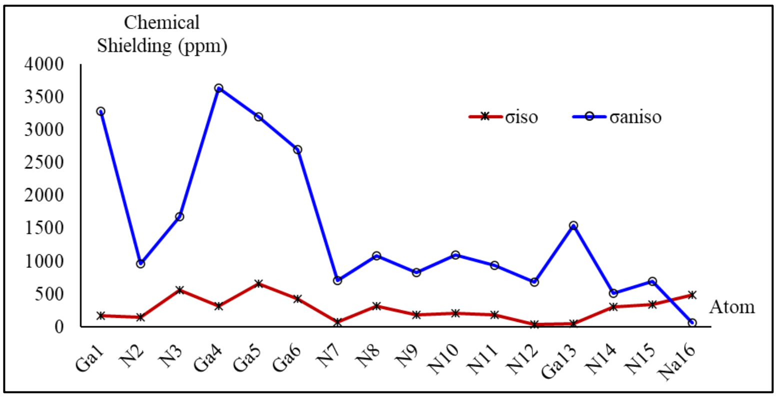

(a)

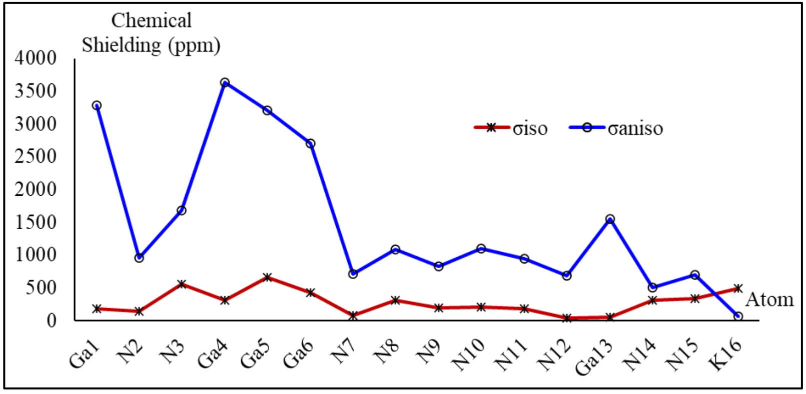

(b)

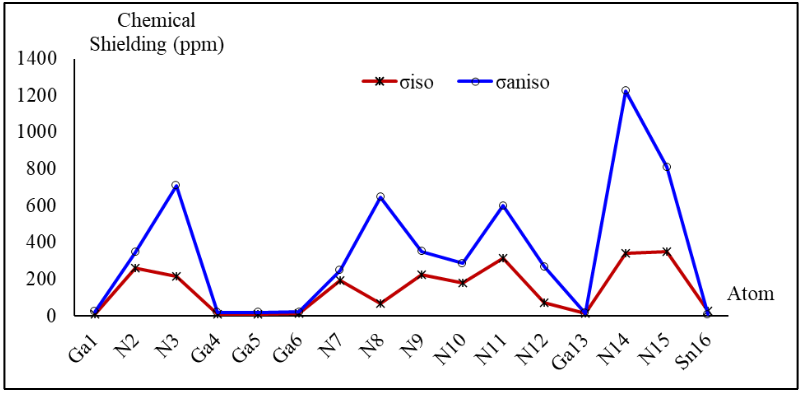

(c)

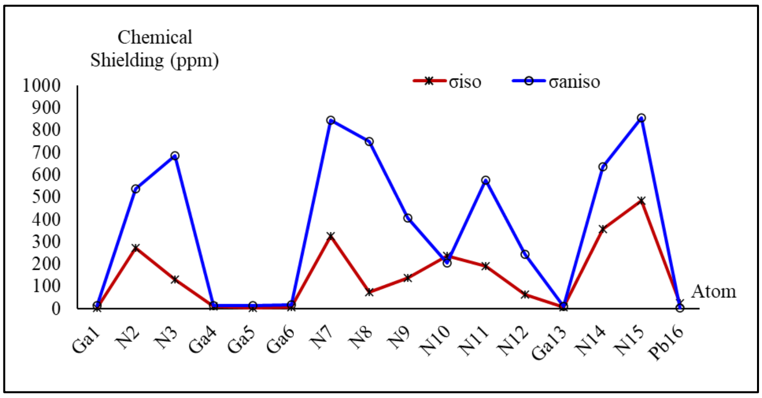

(d)

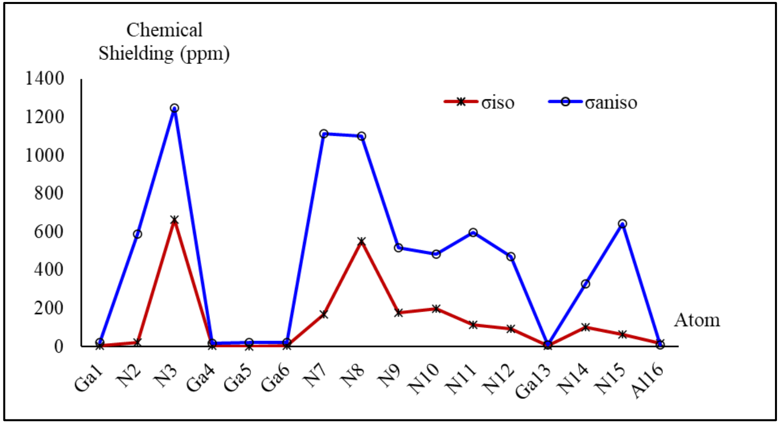

(e)

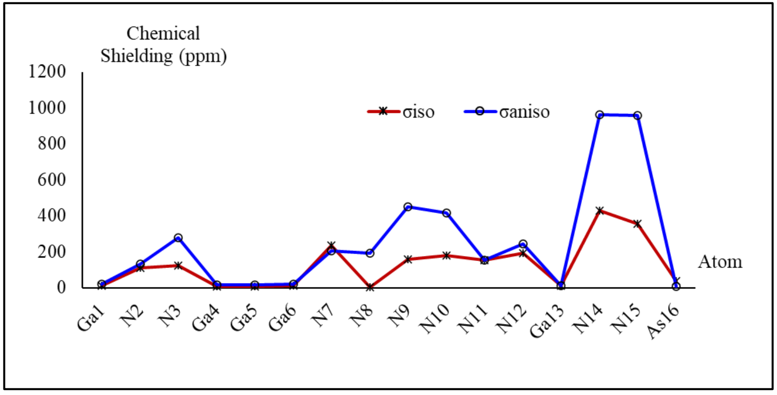

(f)

Figure 3. The NMR spectra for **(a)** Na^+ΞGa–N; **(b)** K^+ΞGa–N; **(c)** Sn^{2+}ΞGa–N; **(d)** Pb^{2+}ΞGa–N; **(e)** Al^{3+}ΞGa–N; **(f)** As^{3+}ΞGa–N complexes using CAM-B3LYP/LANL2DZ.

In Figure 3 (a–f), metal cations of Na^+, K^+, Sn^{2+}, Pb^{2+}, Al^{3+}, As^{3+} in the complexes of Na^+ΞGa–N, K^+ΞGa–N, Sn^{2+}ΞGa–N, Pb^{2+}ΞGa–N, Al^{3+}ΞGa–N, and As^{3+}ΞGa–N denote the fluctuation in the chemical shielding during ion trapping. In fact, Figure 3 (a–f) indicates the gap in chemical shielding between gallium/nitrogen in Ga_5N_{10} nanocage and metal cations. Therefore, it can be considered that the efficiency of electron-accepting for the trapped metal cations in the Ga–N is $K^+ > Na^+ >>> As^{3+} > Sn^{2+} \approx Pb^{2+} > Al^{3+}$ indicates the power of the covalent bond between gallium/nitrogen and these metal cations towards ion removal. In the NMR spectroscopy, it has been observed the remarkable peaks around metal elements of Na^+, K^+, Sn^{2+}, Pb^{2+}, Al^{3+}, and As^{3+} through the trapping in the Ga–N during ion detection and removal from water; however, there are some fluctuations in the chemical shielding behaviors of isotropic and anisotropy attributes.

Therefore, the authors believe that the extracted results would be useful in designing Ga–N based nanomaterials for encapsulating first-group and second-group metals cations of the periodic table in addition to the structural studies using solid-state and solution NMR techniques.

3.3. IR spectroscopy and thermodynamic factors.

The IR calculations have been accomplished to trap metal cations of Na^+, K^+, Sn^{2+}, Pb^{2+}, Al^{3+}, and As^{3+} in the Ga–N during ion sensing in water. Therefore, it has been simulated the several clusters containing Na^+ΞGa–N (Figure 4a), K^+ΞGa–N (Figure 4b), Sn^{2+}ΞGa–N (Figure 4c), Pb^{2+}ΞGa–N (Figure 4d), Al^{3+}ΞGa–N (Figure 4e), and As^{3+}ΞGa–N (Figure 4f).

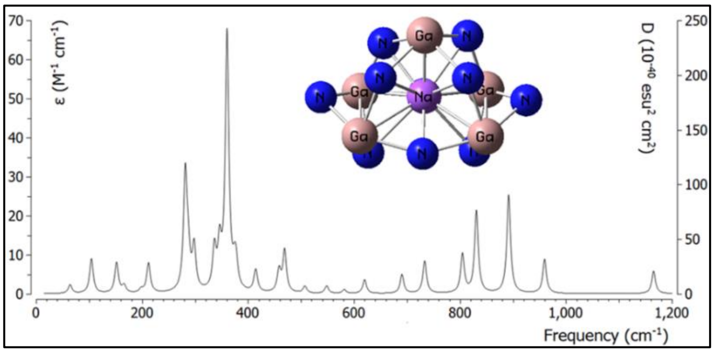

(a)

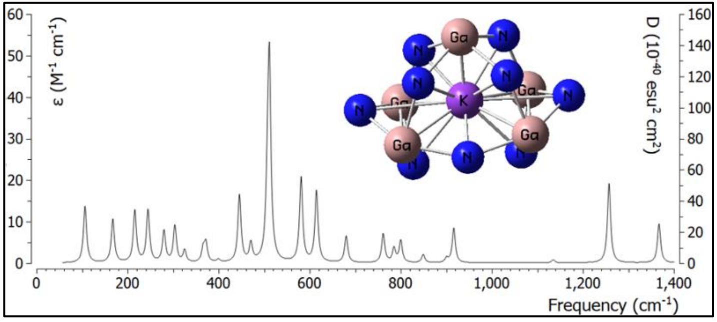

(b)

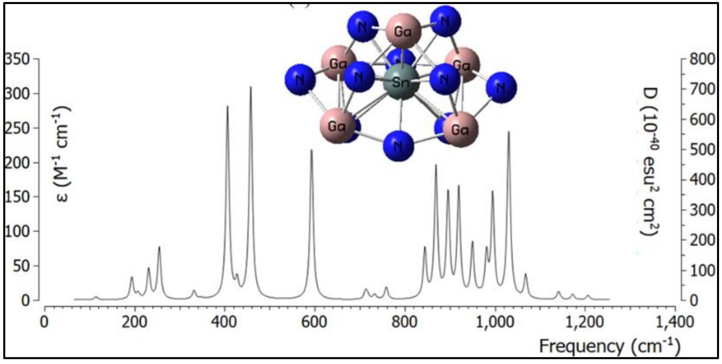

(c)

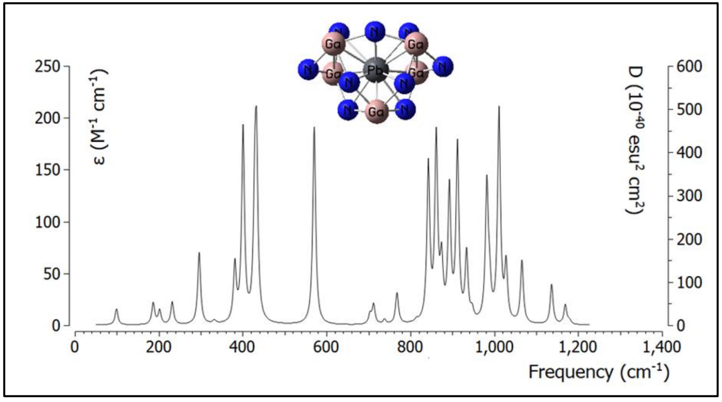

(d)

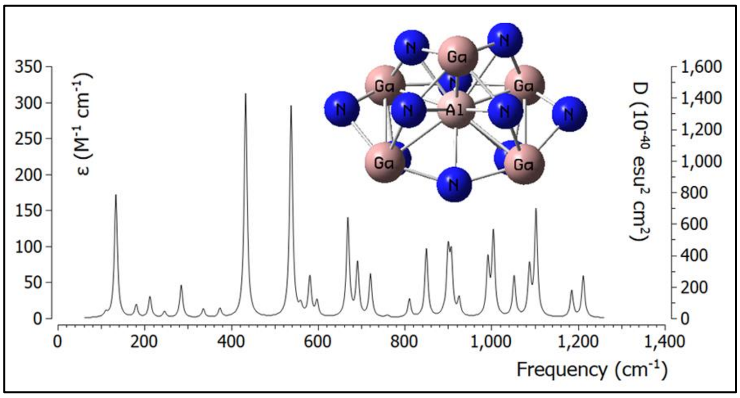

(e)

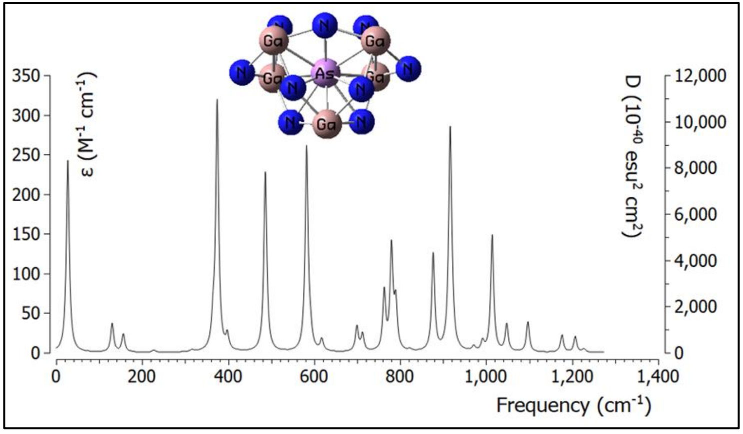

(f)

Figure 4. The Frequency (cm^{-1}) changes through the IR spectra for **(a)** Na^+ΞGa–N; **(b)** K^+ΞGa–N; **(c)** Sn^{2+}ΞGa–N; **(d)** Pb^{2+}ΞGa–N; **(e)** Al^{3+}ΞGa–N; **(f)** As^{3+}ΞGa–N complexes. ε ($M^{-1}cm^{-1}$ or $Lmol^{-1}cm^{-1}$) is the absorbance unit, and D (10^{-4} esu^2 cm^2) is the dipole strength via the esu or electrostatic unit, which is a unit of charge in the cgs (centimeter-gram-second) system.

Figure 4 (a) shows the frequency range between 100–1150 cm^{-1} for Na^+ΞGa–N with sharp peaks around 281.61, 360.46, and 891.95 cm^{-1}. Figure 4 (b) indicates the fluctuation of frequency between 100–1400 cm^{-1} for K^+ΞGa–N with two sharp peaks around 511.8 and 1257.49 cm^{-1}. Moreover, Figure 4 (c) has exhibited the frequency between 200–1200 for Sn^{2+}ΞGa–N with sharp peaks around 254.94,406.60, 458.02, 593.13, 869.27, 919.83, 995.17, and 1030.76 cm^{-1}. Figure 4d has observed the frequency between 200–1200 for Pb^{2+}ΞGa–N with sharp peaks around 400.93, 570.63, 861.70, and 1011.39 cm^{-1}. Furthermore, the frequency between 100–1200 for Al3+ΞGa–N has been observed with sharp peaks around 134.04, 433.33, 538.19, 669.13 and 1103.08 cm^{-1} Figure 4e, Figure 4f has exhibited the frequency between 20–1200 for As^{3+}ΞGa–N with sharp peaks around 27.03, 374.38, 486.44, 582.38, 916.47, and 1013.89 cm^{-1}.

The IR spectra of metal/loid ion complexes with Ga–N have demonstrated that the structure of the dominant complex correlates with the ability of the ion and its size to be adsorbed through Ga–N. As it has been seen, K^+Ξ Ga–N and Na^+ΞGa–N with more electron-accepting properties have the most fluctuations through the adsorption process (Figure 4a and d). Therefore, it can be found that IR spectroscopy of (Na^+, K^+, Sn^{2+}, Pb^{2+}, Al^{3+}, As^{3+})–encapsulated Ga–N is now well-placed to address specific questions on the individual effect of charge carriers (nanocage and ions), as well as solvent molecules on the overall structure (Figure 4 a–f).

Table 3, through thermodynamic specifications, concluded that Ga–N, due to encapsulation of metal cations, including Na^{+}, K^{+}, Sn^{2+}, Pb^{2+}, Al^{3+}, and As^{3+}, might be a more efficient sensor for detecting and removing the ions from water.

Table3. The thermodynamic characters of Na^{+}ΞGa–N , K^{+}ΞGa–N , Sn^{2+}Ξ Ga–N , Pb^{2+}ΞGa–N , Al^{3+}ΞGa–N , and As^{3+}ΞGa–N complexes using CAM-B3LYP/6-311+G (d,p), LANL2DZ calculation.

Compound	**Dipole moment (Debye)**	**$\Delta E^{o}\times10^{-4}$ (kcal/mol)**	**$\Delta H^{o}\times10^{-4}$ (kcal/mol)**	**$\Delta G^{o}\times10^{-4}$ (kcal/mol)**	**S^{o} (cal/K.mol)**
Na^{+}ΞGa–N	0.3167	–640.725	–640.724	–640.728	110.521
K^{+}ΞGa–N	0.5338	–667.875	–667.875	–667.877	99.927
Sn^{2+}ΞGa–N	1.0001	–350.694	–350.693	–350.723	98.834
Pb^{2+}ΞGa–N	0.5613	–350.642	–350.641	–350.671	99.455
Al^{3+}ΞGa–N	0.4854	–350.161	–350.161	–350.190	99.281
As^{3+}ΞGa–N	1.4012	–352.313	–352.313	–352.343	102.904

Thermodynamic parameters of complexes of monovalent (M^{+}), divalent (M^{2+}), and trivalent (M^{3+}) cations with Ga–N have been determined using the DFT theoretical technique. It has been shown that for a given number of nitrogen donor sites in Ga–N, the stabilities of M^{+}, M^{2+}, and M^{3+} complexes are K^{+}ΞGa–N > Na^{+}ΞGa–N >>> As^{3+}ΞGa–N > Sn^{2+}ΞGa–N ≈ Pb^{2+}ΞGa–N > Al^{3+}ΞGa–N (Table 3).

The thermodynamic data in Figure 5 could detect the maximum efficiency of metal cations (Na^{+}, K^{+}, Sn^{2+}, Pb^{2+}, Al^{3+}, As^{3+}) trapped in the Ga–N through ΔG^{o}_{ads} which depends on the covalent bond between the first and second main group metal cations and Ga–N as a potent sensor for water treatment.

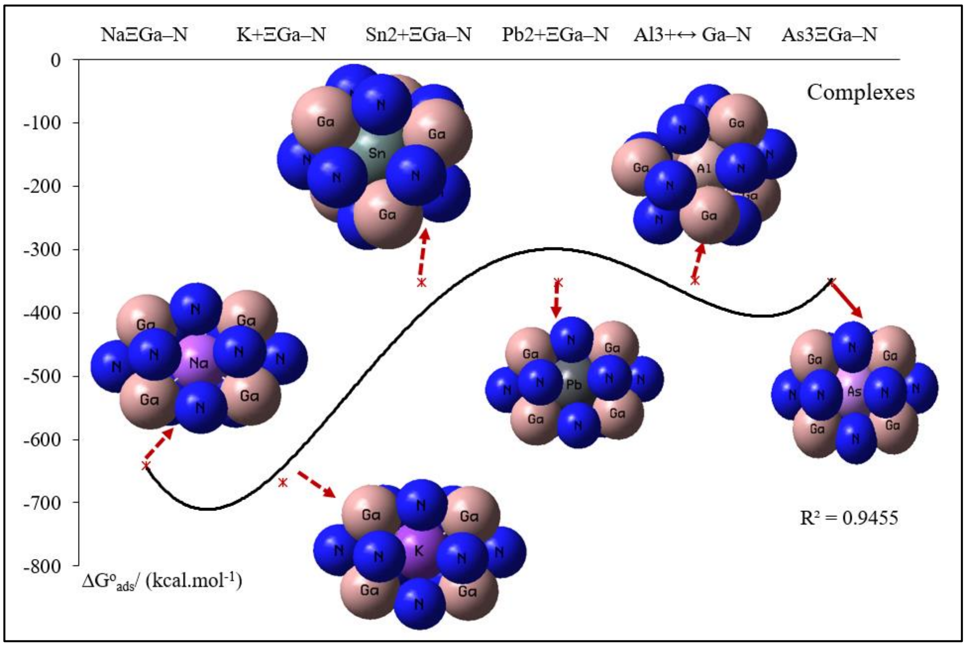

Figure 5. Gibbs free energy (ΔG^{o}_{ads}) for Na^{+}ΞGa–N, K^{+}ΞGa–N, Sn^{2+}ΞGa–N, Pb^{2+}ΞGa–N, Al^{3+}ΞGa–N, and As^{3+}ΞGa–N complexes using CAM-B3LYP/6-311+G (d,p), LANL2DZ.

The encapsulation process of metal cations (Na^{+}, K^{+}, Sn^{2+}, Pb^{2+}, Al^{3+}, As^{3+}) in Ga–N is affirmed by the ΔG^{o}_{ads} quantities:

$$\Delta G^{o}_{ads} = \Delta G^{o}_{Ion\Xi Ga-N} - \left(\Delta G^{o}_{Ion-trapped} + \Delta G^{o}_{Ga-N}\right) \qquad (13)$$

Ions= $Na^{+},K^{+},Sn^{2+},Pb^{2+},Al^{3+},As^{3+}$ (14)

As seen in Table 3, all the accounted ΔG^{o}_{ads} amounts are very close, demonstrating the agreement of the measured specifications by all methodologies and the reliability of the computing values.

Figure 6 shows the dependence on the size of the ions during interaction between the adsorbates of the alkali and alkaline earth metals cations as the electron acceptors and the adsorbent of Ga–N as electron donor in the complexes of Na^{+}ΞGa–N, K^{+}ΞGa–N, Sn^{2+}ΞGa–N, Pb^{2+}ΞGa–N, Al^{3+}ΞGa–N, and As^{3+}ΞGa–N. Therefore, the selectivity of metal ions by gallium nitride nanocage (ion sensor) can result in $K^{+}>Na^{+}>>>As^{3+}>Sn^{2+}\approx Pb^{2+}>Al^{3+}$ (Table 3 and Figure 5).

All in all, adsorption involving charged adsorbed species causes a change in the double layer and the potential at the outer Helmholtz plane, influencing the storage rates of both anodic and cathodic reactions. The first three modes are intimate with adsorption and the double layer. The last involves the interaction of the metal cations trapping and the intermediate products formed during the partial electrochemical reactions. Interaction of the adsorbed intermediates with metal cations can either decrease or increase the electrode reaction rate depending on the stability of the metal cation-intermediate complex formed.

4. Conclusions

Gallium nitride nanocage (Ga–N) can effectively remove metal/loid ions from water. Ion separation involving a gallium nitride nanocage (Ga–N) can be used to remove a series of cations from aqueous solutions based on electrostatic interactions between the metal cations and Ga–N.

The electromagnetic and thermodynamic properties of metal/metalloid adsorbed Ga–N systems were investigated using density functional theory. The results have illustrated that all the metal/metalloid adsorbed Ga–N are rather stable, with the most stable adsorption site being in the center of the Ga–N system. The selectivity of metal ions by gallium nitride nanocage (ion sensor) can be resulted as: $K^{+}>Na^{+}>>>As^{3+}>Sn^{2+}\approx Pb^{2+}>Al^{3+}$. Thus, it was indicated that for a given number of nitrogen donor sites in Ga–N, the stabilities of M^{+} are higher than M^{2+} and M^{3+} complexes as K^{+}ΞGa–N > Na^{+}ΞGa–N>>>As^{3+}ΞGa–N>Sn^{2+}ΞGa–N≈Pb^{2+}ΞGa–N>Al^{3+}ΞGa–N. Moreover, it is proposed that metal/metalloid–absorbed can be used to decorate and enlarge the optoelectronic properties of Ga–N, which can be used to produce photoelectric devices [78].

Author Contributions

Conceptualization, F.M.; methodology, F.M.; software F.M.; validation, F.M.; formal analysis, F.M.; investigation, F.M.; resources, F.M.; data curation, F.M.; writing—original draft preparation, F.M.; writing—review and editing, F.M.; visualization, F.M.; supervision, F.M.; project administration, F.M.; funding acquisition, F.M.The author has read and agreed to the published version of the manuscript.

Institutional Review Board Statement

Not applicable.

Informed Consent Statement

Not applicable.

Data Availability Statement

Data supporting the findings of this study are available upon reasonable request from the corresponding author.

Funding

This research received no funding.

Acknowledgments

The author is grateful to Kastamonu University for successfully completing this paper and its research.

Conflict of Interest

The author declares no conflict of interest.

References

1. Lajoie, L.; Fabiano-Tixier, A.-S.; Chemat, F. Water as Green Solvent: Methods of Solubilisation and Extraction of Natural Products—Past, Present and Future Solutions. *Pharmaceuticals* **2022**, *15*, 1507, https://doi.org/10.3390/ph15121507.
2. Wang, M.; Wang, Z.; Zhang, J.; Zhan, J.; Wu, C.; Yu, W.; Fan, W.; Tang, J.; Zhang, Q.; Zhang, J. Sustainable Bioactive Salts Fully Composed of Natural Products for Enhanced Pharmaceutical Applicability. *ACS Sustainable Chem. Eng.* **2022**, *10*, 10369-10382, https://doi.org/10.1021/acssuschemeng.2c03138.
3. Micheau, C.; Schneider, A.; Girard, L.; Bauduin, P. Evaluation of ion separation coefficients by foam flotation using a carboxylate surfactant. *Colloids Surf. A: Physicochem. Eng. Asp.* **2015**, *470*, 52-59, https://doi.org/10.1016/j.colsurfa.2015.01.049.
4. Ghosh, R.; Sahu, A.; Pushpavanam, S. Removal of trace hexavalent chromium from aqueous solutions by ion foam fractionation. *J. Hazard. Mater.* **2019**, *367*, 589-598, https://doi.org/10.1016/j.jhazmat.2018.12.105.
5. Matsuoka, K.; Miura, H.; Karima, S.; Taketaka, C.; Ouno, S.; Moroi, Y. Removal of alkali metal ions from aqueous solution by foam separation method. *J. Mol. Liq.* **2018**, *263*, 89-95, https://doi.org/10.1016/j.molliq.2018.04.136.
6. Lindblom, G.; Lindman, B.; Tiddy, G.J.T. Ion binding studied using quadrupole splittings of sodium-23(1+) ions in lyotropic liquid crystals. The dependence on surfactant type. *J. Am. Chem. Soc.* **1978**, *100*, 2299-2303, https://doi.org/10.1021/ja00476a005.
7. Leigh, I.D.; McDonald, M.P.; Wood, R.M.; Tiddy, G.J.T.; Trevethan, M.H. Structure of liquid-crystalline phases formed by sodium dodecyl sulphate and water as determined by optical microscopy, X-ray diffraction and nuclear magnetic resonance spectroscopy. J. *Chem. Soc. Faraday Trans.* **1981**, *77*, 2867-2876, https://doi.org/10.1039/F19817702867.
8. Schwierz, N.; Horinek, D.; Netz, R.R. Reversed Anionic Hofmeister Series: The Interplay of Surface Charge and Surface Polarity. *Langmuir* **2010**, *26*, 7370-7379, https://doi.org/10.1021/la904397v.
9. Ropers, M.H.; Czichocki, G.; Brezesinski, G. Counterion Effect on the Thermodynamics of Micellization of Alkyl Sulfates. *J. Phys. Chem. B* **2003**, *107*, 5281-5288, https://doi.org/10.1021/jp0264329.
10. Mollaamin, F. Competitive Intracellular Hydrogen-Nanocarrier Among Aluminum, Carbon, or Silicon Implantation: a Novel Technology of Eco-Friendly Energy Storage using Research Density Functional Theory. *Russ. J. Phys. Chem. B.* **2024**, *18*, 805-820, https://doi.org/10.1134/S1990793124700131.
11. adatshojaei, E.; Wood, D.A. Chapter 15 - Water, the most accessible eco-friendly solvent, and extraction and separation agent. In Green Sustainable Process for Chemical and Environmental Engineering and Science,

Inamuddin, Boddula, R., Asiri, A.M., Eds.; Elsevier: **2021**; pp. 283-292, https://doi.org/10.1016/B978-0-12-821884-6.00012-7.

12. Cheng, Y.; Xue, F.; Yu, S.; Du, S.; Yang, Y. Subcritical Water Extraction of Natural Products. *Molecules* **2021**, *26*, 4004, https://doi.org/10.3390/molecules26134004.
13. Mollaamin, F.; M. Monajjemi, Nanomaterials for Sustainable Energy in Hydrogen-Fuel Cell: Functionalization and Characterization of Carbon Nano-Semiconductors with Silicon, Germanium, Tin or Lead through Density Functional Theory Study. *Russ. J. Phys. Chem. B.* **2024**, *18*, 607-623, https://doi.org/10.1134/S1990793124020271.
14. Hiratsuka, A.; Yasuda, Y. Study on the Possibility of Mixed Water as a Drinking Water—From the Viewpoint of the Formation of Hydrogen-Rich Water. *J. Water Resour. Prot.* **2021**, *13*, 44-73, https://doi.org/10.4236/jwarp.2021.131004.
15. Gidlow, D.A. Lead toxicity. *Occup. Med.* **2015**, *65*, 348-356, https://doi.org/10.1093/occmed/kqv018.
16. Vincent, T.; Krys, P.; Jouannin, C.; Gaumont, A.C.; Dez, I.; Guibal, E. Hybrid macroporous Pd catalytic discs for 4-nitroaniline hydrogenation: Contribution of the alginate-tetraalkylphosphonium ionic liquid support. *J. Organomet. Chem.* **2013**, *723*, 90-97, https://doi.org/10.1016/j.jorganchem.2012.10.008.
17. Czulak, J.; C., J.; T., V.; I., D.; C., G.A.; and Guibal, E. Nitrophenol Hydrogenation Using Pd Immobilized on Ionic Liquid-Alginate Spherical Resins. *Sep. Sci. Technol.* **2012**, *47*, 2166-2176.
18. Singh, R.; Gautam, N.; Mishra, A.; Gupta, R. Heavy metals and living systems: An overview. *Indian J Pharmacol* **2011**, *43*, 246-253, https://doi.org/10.4103/0253-7613.81505.
19. Zhang, S.; Gao, H.; Li, J.; Huang, Y.; Alsaedi, A.; Hayat, T.; Xu, X.; Wang, X. Rice husks as a sustainable silica source for hierarchical flower-like metal silicate architectures assembled into ultrathin nanosheets for adsorption and catalysis. *J. Hazard. Mater.* **2017**, *321*, 92-102, https://doi.org/10.1016/j.jhazmat.2016.09.004.
20. Jain, R. Recent advances of magnetite nanomaterials to remove arsenic from water. *RSC Adv.* **2022**, *12*, 32197–32209, https://doi.org/10.1039/d2ra05832d.
21. Rybarczyk, P.; Kawalec-Pietrenko, B. Simultaneous Removal of Al, Cu and Zn Ions from Aqueous Solutions Using Ion and Precipitate Flotation Methods. *Processes* **2021**, *9*, 301, https://doi.org/10.3390/pr9020301.
22. Rathinam, B.; Murugesan, V.; Liu, B.-T. Fluorescent “OFF–ON” Sensors for the Detection of Sn^{2+} Ions Based on Amine-Functionalized Rhodamine 6G. *Chemosensors* **2022**, *10*, 69, https://doi.org/10.3390/chemosensors10020069.
23. Mollaamin, F.; Monajjemi, M. Doping of Graphene Nanostructure with Iron, Nickel and Zinc as Selective Detector for the Toxic Gas Removal: A Density Functional Theory Study. *C–Journal of Carbon Research.* **2023**, *9*, 20, https://doi.org/10.3390/c9010020.
24. Mollaamin, F.; Monajjemi, M. Structural, Electromagnetic and Thermodynamic Analysis of Ion Pollutants Adsorption in Water by Gallium Nitride Nanomaterial: a Green Chemistry Application. *Russ. J. Phys. Chem. B.* **2024**, *18*, 533-548, https://doi.org/10.1134/S199079312402012X.
25. Mollaamin, F.; Monajjemi, M. Tribocorrosion Framework of (Iron, Nickel, Zinc)-Doped Graphene Nanosheet: New Sights into Sulfur Dioxide and Hydrogen Sulfide Removal Using DFT/TD-DFT Methods. *J. Bio Tribo-Corros.* **2023**, *9*, 47, https://doi.org/10.1007/s40735-023-00768-3.
26. Mollaamin, F. Computational Methods in the Drug Delivery of Carbon Nanocarriers onto Several Compounds in Sarraceniaceae Medicinal Plant as Monkeypox Therapy. *Computation*. **2023**, *11*, 84, https://doi.org/10.3390/computation11040084.
27. Mollaamin, F.; Monajjemi, M. Trapping of toxic heavy metals from water by GN–nanocage: Application of nanomaterials for contaminant removal technique. *J. Mol. Struct.* **2024**, *1300*, 137214, https://doi.org/10.1016/j.molstruc.2023.137214.
28. Mollaamin, F. Features of parametric point nuclear magnetic resonance of metals implantation on boron nitride nanotube by density functional theory/electron paramagnetic resonance. *J. Comput. Theor. Nanosci.* **2024**, *11*, 2393-2398, https://doi.org/10.1166/jctn.2014.3653.
29. Ikawa, Y.; Lee, K.; Ao, J.-P.; Ohno, Y. Two-dimensional device simulation of AlGaN/GaN heterojunction FET side-gating effect. *Jpn. J. Appl. Phys.* **2014**, *53*, 114302, https://doi.org/10.7567/JJAP.53.114302.
30. Podolska, A.; Seeber, R.M.; Mishra, U.K.; Pfleger, K.D.G.; Parish, G.; Nener, B.D. Detection of biological reactions by AlGaN/GaN biosensor. In Proceedings of the COMMAD 2012, Melbourne, VIC, Australia, 12-14 Dec. 2012; IEEE:**2012**; pp. 75-76, https://doi.org/10.1109/COMMAD.2012.6472367.

31. Prokopuk, N.; Kyung-Ah, S.; George, T.; Moon, J.S. Development of GaN-based micro chemical sensor nodes. In Proceedings of the SENSORS, Irvine, CA, USA, 2005 IEEE, 30 Oct.-3 Nov. 2005; IEEE: **2005**; p. 4, https://doi.org/10.1109/ICSENS.2005.1597670.
32. Pearton, S.J.; Kang, B.S.; Suku, K.; Ren, F.; Gila, B.P.; Abernathy, C.R.; Jenshan, L.; Chu, S.N.G. GaN-based diodes and transistors for chemical, gas, biological and pressure sensing. *J. Phys.: Condens. Matter* **2004**, *16*, R961, https://doi.org/10.1088/0953-8984/16/29/R02.
33. Mollaamin, F.; Monajjemi, M. Graphene Embedded with Transition Metals for Capturing Carbon Dioxide: Gas Detection Study Using QM Methods. *Clean Technologies.* **2023**, *5*, 403-417, https://doi.org/10.3390/cleantechnol5010020.
34. Yong, Y.; Cui, H.; Zhou, Q.; Su, X.; Kuang, Y.; Li, X. Adsorption of gas molecules on a graphitic GaN sheet and its implications for molecule sensors. *RSC Adv.* **2017**, *7*, 51027-51035, https://doi.org/10.1039/c7ra11106a.
35. Khan, M.A.H.; Rao, M.V. Gallium Nitride (GaN) Nanostructures and Their Gas Sensing Properties: A Review. *Sensors* **2020**, *20*, 3889, https://doi.org/10.3390/s20143889.
36. Mollaamin, F.; Monajjemi, M. Tailoring and functionalizing the graphitic-like GaN and GaP nanostructures as selective sensors for NO, NO_2, and NH_3 adsorbing: a DFT study. *J. Mol. Model.* **2023**, *29*, 170, https://doi.org/10.1007/s00894-023-05567-8.
37. Bakhshi, K.; Mollaamin, F.; Monajjemi, M. Exchange and Correlation Effect of Hydrogen Chemisorption on Nano V(100) Surface: A DFT Study by Generalized Gradient Approximation (GGA). *J. Comput. Theor. Nanosci.* **2011**, *8*, 763-768, https://doi.org/10.1166/jctn.2011.1750.
38. Mollaamin, F.; Monajjemi, M. Electric and Magnetic Evaluation of Aluminum–Magnesium Nanoalloy Decorated with Germanium Through Heterocyclic Carbenes Adsorption: A Density Functional Theory Study. *Russ. J. Phys. Chem.* **2023**, *17*, 658-672, https://doi.org/10.1134/s1990793123030223.
39. Mollaamin, F.; Monajjemi, M. Corrosion Inhibiting by Some Organic Heterocyclic Inhibitors Through Langmuir Adsorption Mechanism on the Al-X (X = Mg/Ga/Si) Alloy Surface: A Study of Quantum Three-Layer Method of CAM-DFT/ONIOM. *J. Bio- Tribo-Corros.* **2023**, *9*, 33, https://doi.org/10.1007/s40735-023-00751-y.
40. Strite, S.; Morkoç, H. GaN, AlN, and InN: A review. *J. Vac. Sci. Technol. B* **1992**, *10*, 1237-1266, https://doi.org/10.1116/1.585897.
41. Monemar, B. III-V nitrides—important future electronic materials. *J. Mater. Sci. Mater. Electronics* **1999**, *10*, 227–254, https://doi.org/10.1023/A:1008991414520.
42. Cui, Z.; Li, E.; Ke, X.; Zhao, T.; Yang, Y.; Ding, Y.; Liu, T.; Qu, Y.; Xu, S. Adsorption of alkali-metal atoms on GaN nanowires photocathode. *Appl. Surf. Sci.* **2017**, *423*, 829-835, https://doi.org/10.1016/j.apsusc.2017.06.233.
43. Mollaamin, F.; Monajjemi, M. Transition metal (X = Mn, Fe, Co, Ni, Cu, Zn)-doped graphene as gas sensor for CO_2 and NO_2 detection: a molecular modeling framework by DFT perspective. *J. Mol. Model.* **2023**, *29*, 119, https://doi.org/10.1007/s00894-023-05526-3.
44. Jin, K.-H.; Choi, S.-M.; Jhi, S.H. Crossover in the adsorption properties of alkali metals on graphene. *Phys. Rev. B* **2010**¸*82*, 033414, https://doi.org/10.1103/PhysRevB.82.033414.
45. Mollaamin, F.; Monajjemi, M. Fractal dimension on carbon nanotube-polymer composite materials using percolation theory. *J. Comput. Theor. Nanosci.* **2012**, *9*, 597-601, https://doi.org/10.1166/jctn.2012.2067.
46. Ding, Y.; Wang, Y. Structural, Electronic, and Magnetic Properties of Adatom Adsorptions on Black and Blue Phosphorene: A First-Principles Study. *J. Phys. Chem. C* **2015**, *119*, 10610-10622, https://doi.org/10.1021/jp5114152.
47. Mollaamin, F.; Monajjemi, M. Graphene-based resistant sensor decorated with Mn, Co, Cu for nitric oxide detection: Langmuir adsorption & DFT method. *Sensor Rev.* **2023**, *43*, 266-279, https://doi.org/10.1108/SR-03-2023-0040.
48. Khalili Hadad, B.; Mollaamin, F.; Monajjemi, M. Biophysical chemistry of macrocycles for drug delivery: a theoretical study. *Russ. Chem. Bull.* **2011**, *60*, 238-241, https://doi.org/10.1007/s11172-011-0039-5.
49. Mollaamin, F.; Monajjemi, M. In Silico-DFT Investigation of Nanocluster Alloys of Al-(Mg, Ge, Sn) Coated by Nitrogen Heterocyclic Carbenes as Corrosion Inhibitors. *J. Clust. Sci.* **2023**, *34*, 2901-2918, https://doi.org/10.1007/s10876-023-02436-5.
50. Jiang, J.; Liang, Q.; Meng, R.; Yang, Q.; Tan, C.; Sun, X.; Chen, X. Exploration of new ferromagnetic, semiconducting and biocompatible Nb_3X_8 (X = Cl, Br or I) monolayers with considerable visible and infrared light absorption. *Nanoscale* **2017**, *9*, 2992-3001, https://doi.org/10.1039/C6NR07231C.

51. Mollaamin, F.; Shahriari, S.; Monajjemi, M.; Khalaj, Z. Nanocluster of Aluminum Lattice via Organic Inhibitors Coating: A Study of Freundlich Adsorption. *J. Clust. Sci.* **2022**, *34*, 1547-1562, https://doi.org/10.1007/s10876-022-02335-1.
52. Mollaamin, F.; Monajjemi, M.; Shojaei, S. An overview on Coronaviruses family from past to Covid-19: introduce some inhibitors as antiviruses from Gillan's plants. *Biointerface Res. Appl. Chem.* **2020**, *10*, 5575-5585, https://doi.org/10.33263/BRIAC103.575585.
53. Mollaamin, F.; Monajjemi, M. Molecular modelling framework of metal-organic clusters for conserving surfaces: Langmuir sorption through the TD-DFT/ONIOM approach. *Mol. Simul.* **2023**, *49*, 365-376, https://doi.org/10.1080/08927022.2022.2159996.
54. Cui, Z.; Wang, X.; Li, E.; Ding, Y.; Sun, C.; Sun, M. Alkali-metal-adsorbed g-GaN monolayer: ultralow work functions and optical properties. *Nanoscale Res. Lett.* **2018**, *13*, 207, https://doi.org/10.1186/s11671-018-2625-z.
55. Roy, R.S.; Mondal, A.; Nandi, P.K. First hyperpolarizability of cyclooctatetraene modulated by alkali and alkaline earth metals. *J. Mol. Model.* **2017**, *23*, 93, https://doi.org/10.1007/s00894-017-3273-4.
56. Henkelman, G.; Arnaldsson, A.; Jónsson, H. A fast and robust algorithm for Bader decomposition of charge density. *Comput. Mater. Sci.* **2006**, *36*, 354-360, https://doi.org/10.1016/j.commatsci.2005.04.010.
57. Mollaamin, F.; Monajjemi, M. DFT outlook of solvent effect on function of nano bioorganic drugs. *Phys. Chem. Liq.* **2012**, *50*, 596-604, https://doi.org/10.1080/00319104.2011.646444.
58. Perdew, J.P.; Burke, K.; Ernzerhof, M. Generalized Gradient Approximation Made Simple. *Phys. Rev. Lett.* **1996**, *77*, 3865, https://doi.org/10.1103/PhysRevLett.77.3865.
59. Ziesche, P.; Kurth, S.; Perdew, J.P. Density functionals from LDA to GGA. *Comput. Mater. Sci.* **1998**, *11*, 122–127, https://doi.org/10.1016/S0927-0256(97)00206-1.
60. Arrigoni, M.; Madsen, G.K.H. Comparing the performance of LDA and GGA functionals in predicting the lattice thermal conductivity of III-V semiconductor materials in the zincblende structure: The cases of AlAs and BAs. *Comput. Mater. Sci.* **2019**, *156*, 354–360, https://doi.org/10.1016/j.commatsci.2018.10.005.
61. Hohenberg, P.; Kohn, W. Inhomogeneous Electron Gas. *Phys. Rev. B* **1964**, *136*, B864, https://doi.org/10.1103/PhysRev.136.B864.
62. Kohn, W.; Sham, L.J. Self-Consistent Equations Including Exchange and Correlation Effects. *Phys. Rev.* **1965**, *140*, A1133, https://doi.org/10.1103/PhysRev.140.A1133.
63. Becke, A.D. Density-functional thermochemistry. III. The role of exact exchange. *J. Chem. Phys.* **1993**, *98*, 5648–5652, https://doi.org/10.1063/1.464913.
64. Lee, C.; Yang, W.; Parr, R.G. Development of the Colle–Salvetti correlation-energy formula into a functional of the electron density. *Phys. Rev. B* **1988**, *37*, 785, https://doi.org/10.1103/PhysRevB.37.785.
65. Kim, K.; Jordan, K.D. Comparison of Density Functional and MP2 Calculations on the Water Monomer and Dimer. *J. Phys. Chem.* **1994**, *98*, 10089–10094, https://doi.org/10.1021/j100091a024.
66. Stephens, P.J.; Devlin, F.J.; Chabalowski, C.F.; Frisch, M.J. Ab Initio Calculation of Vibrational Absorption and Circular Dichroism Spectra Using Density Functional Force Fields. *J. Phys. Chem.* **1994**, *98*, 11623-11627, https://doi.org/10.1021/j100096a001.
67. Cramer, C.J. Essentials of Computational Chemistry: Theories and Models, 2nd Edition; Wiley, **2004**.
68. Mollaamin, F.; Monajjemi, M. In Situ Ti-Embedded SiC as Chemiresistive Nanosensor for Safety Monitoring of CO, CO_2, NO, NO_2: Molecular Modelling by Conceptual Density Functional Theory. *Russ. J. Phys. Chem. B.* **2024**, *18*, 49-66, https://doi.org/10.1134/S1990793124010159.
69. Mollaamin, F.; Monajjemi, M. Adsorption ability of Ga_5N_{10} nanomaterial for removing metal ions contamination from drinking water by DFT. *Int. J. Quantum Chem.* **2024**, *124*, e27348, https://doi.org/10.1002/qua.27348.
70. Vosko, S.H.; Wilk, L.; Nusair, M. Accurate spin-dependent electron liquid correlation energies for local spin density calculations: a critical analysis. *Can. J. Phys.* **1980**, *58*, 1200–1211, https://doi.org/10.1139/p80-159.
71. Frisch, M.J.; Trucks, G.W.; Schlegel, H.B.; Scuseria, G.E.; Robb, M.A.; Cheeseman, J.R.; Scalmani, G.; Barone, V.; Petersson, G.A.; Nakatsuji, H.; Li, X.; Caricato, M.; Marenich, A.V.; Bloino, J.; Janesko, B.G.; Gomperts, R.; Mennucci, B.; Hratchian, H.P.; Ortiz, J. V.; Izmaylov, A. F.; Sonnenberg, J.L.; Williams-Young, D.; Ding, F.; Lipparini, F.; Egidi, F.; Goings, J.; Peng, B.; Petrone, A.; Henderson, T.; Ranasinghe, D.; Zakrzewski, V.G.; Gao, J.; Rega, N.; Zheng, G.; Liang, W.; Hada, M.; Ehara, M.; Toyota, K.; Fukuda, R.; Hasegawa, J.; Ishida, M.; Nakajima, T.; Honda, Y.; Kitao, O.; Nakai, H.; Vreven, T.; Throssell, K.; Montgomery, J.A., Jr.; Peralta, J.E.; Ogliaro, F.; Bearpark, M.J.; Heyd, J.J.; Brothers, E.N.; Kudin, K.N.; Staroverov, V.N.; Keith, T.A.; Kobayashi, R.; Normand, J.; Raghavachari, K.; Rendell, A.P.; Burant, J.C.;

Iyengar, S.S.; Tomasi, J.; Cossi, M.; Millam, J.M.; Klene, M.; Adamo, C.; Cammi, R.; Ochterski, J.W.; Martin, R.L.; Morokuma, K.; Farkas, O.; Foresman, J.B.; Fox, D.J. Gaussian 16, Revision C.01, Gaussian, Inc., Wallingford CT, **2016**.

72. Dennington, R.; Keith, T.A.; Millam, J.M. GaussView 6.0. 16. Semichem Inc., Shawnee Mission, **2016**.
73. Mollaamin, F.; Monajjemi, M. Carbon Nanotubes as Biosensors for Releasing Conjugated Bisphosphonates–Metal Ions in Bone Tissue: Targeted Drug Delivery through the DFT Method. *C–Journal of Carbon Research.* **2023**, *9*, 61. https://doi.org/10.3390/c9020061.
74. Mollaamin, F. On the behavior of boron nitride Nanotube-Flavin adenine Dinucleotide interaction ion implantation order to design Biofuel cells. *J. Comput. Theor. Nanosci.* **2014**, *11*, 2017-2022, https://doi.org/10.1166/jctn.2014.3601.
75. Mollaamin, F. Investigating the Treatment of Transition Metals for Ameliorating the Ability of Boron Nitride for Gas Sensing & Removing: A Molecular Characterization by DFT Framework. *Prot. Met. Phys. Chem. Surf.* **2024**, *60*,1050-1063, https://doi.org/10.1134/S2070205124702502.
76. Young, H.D.; Freedman, R.A.; Ford, A.L. Sears and Zemansky's University Physics with Modern Physics, 13th Edition; Addison-Wesley: Boston, USA, **2011**.
77. Sohail, U.; Ullah, F.; Binti Zainal Arfan, N.H.; Abdul Hamid, M.H.S.; Mahmood, T.; Sheikh, N.S.; Ayub, K. Transition Metal Sensing with Nitrogenated Holey Graphene: A First-Principles Investigation. *Molecules* **2023**, *28*, 4060, https://doi.org/10.3390/molecules28104060.
78. Pang, R.; Yin, J.; Wang, Y.; Lin, Q.; Wang, Z.; Xu, L.; Hou, S.; Wang, H.; Yin, J.; Yang, T. Theoretical Investigation of Spectroscopic Properties of the Alkaline-Earth-Metal Monohydrides toward Laser Cooling and Magneto-Optical Trapping. *ACS Omega* **2023**, *8*, 19391-19401, https://doi.org/10.1021/acsomega.3c00352.

Publisher’s Note & Disclaimer